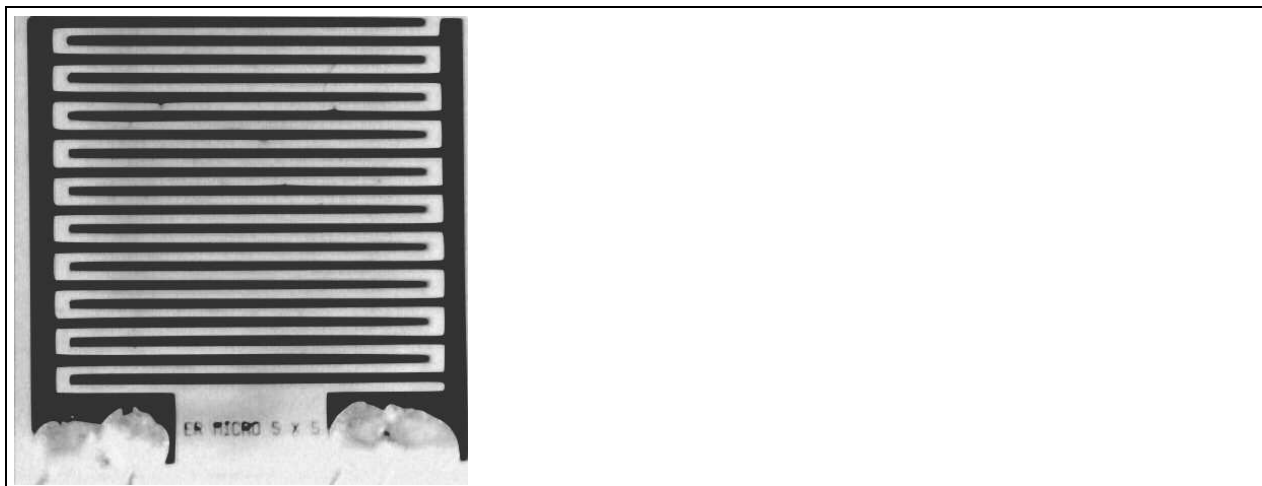# in-situ impedance and morphology of self-assembling gold nanoislands and a method of characterizing size

John Donovan, Dr. Chuhee Kwon

University of California, Long Beach, CA

donovan.csulb@gmail.com ckwon@csulb.edu

April 7, 2015

Contents

Figure 1: The self-assembling gold monolayers are deposited on a gold inter-digitized electrode (IDE).

Introduction

Gold nanoislands may be formed by annealing a substrate – on which gold has been uniformly deposited – to produce islands within a predictable range of size and shape.

This research attempts to characterizes the reproducibility of gold nano-island morphology using the polymer-assisted deposition and self-assembly method.

Prior research suggests that the physical properties of gold nano-islands are sensitive to the method of depositing the gold, the number of layers, and variations in annealing temperature [?].

[The LSPR absorption features of colloidal gold are shown by Kedem and Rubinstein (2011 acs) [add to bibtex, make sure it's original research]

[there is more research to cite here – lots of study of self-assembled islands from evaporative deposition by Van Duyne and his chain of relevant citations show properties vs. size et cetera, and I should find the proper method of citing other people's figures].

Gold nano-island formation through polymer-assisted self-assembly is also sensitive to the initial size of the colloidal gold used to form the self-assembling layers cite(reference), to the temperature profile during annealing, and to the length of time (in days) between creation and annealing ([?]).

[more junk to clean up – if I analyze how the polymer-deposited samples decay in air, it'll be done near the end of my research and be given a single paragraph and one figure]

This research quantifies the repeatiblity of gold nano-islands produced using the label-free(*) self-assembly method.

[quote junk: I want these somewhere]

> Plasmonic nanoparticles also act as transducers that convert small changes in the local refractive index into spectral shifts in the intense nanoparticle extinction and scattering spectra. Most organic molecules have a higher refractive index than buffer solution; thus, when they bind to nanoparticles, the local refractive index increases, causing the extinction and scattering spectrum to redshift. Molecular

TABLE 1. Statistical Data for Morphology of Annealed Gold Island Films

nominal thickness (nm)	coverage (%)	effective height (nm)	average axis (nm) major	average axis (nm) minor	aspect ratio in-plane[a]	aspect ratio out-of-plane[b]	average interparticle distance (nm)	particle surface density (cm^{-2})
3	49.8	6	22.3 ± 4.9	20.1 ± 4.5	1.11 ± 0.08	3.5 ± 0.8	27.3 ± 4.2	1.6 × 10^{11}
4	50.2	8	27.1 ± 6.6	23.8 ± 5.9	1.14 ± 0.10	3.2 ± 0.8	32.6 ± 4.8	9.3 × 10^{10}
5	40.9	12.2	34.2 ± 9.6	31.1 ± 8.7	1.10 ± 0.07	2.7 ± 0.8	46.1 ± 8.9	4.4 × 10^{10}
6	52.0	11.5	39.9 ± 10.6	35.7 ± 10.3	1.14 ± 0.11	3.3 ± 0.9	48.3 ± 7.7	4.2 × 10^{10}
7.5	36.5	20.5	73.5 ± 22.2	64.3 ± 18.2	1.14 ± 0.10	3.4 ± 1.0	105.4 ± 18.8	9.2 × 10^{9}
9	35.1	25.6	79.0 ± 30.4	66.9 ± 23.2	1.17 ± 0.14	2.8 ± 1.0	111.7 ± 22.1	7.3 × 10^{9}
10	31.3	31.9	113.5 ± 41.1	92.4 ± 28.3	1.22 ± 0.17	3.2 ± 1.1	168.7 ± 27.8	2.8 × 10^{9}

[a] Major axis divided by the minor axis. [b] Average of major and minor axes divided by the effective height.
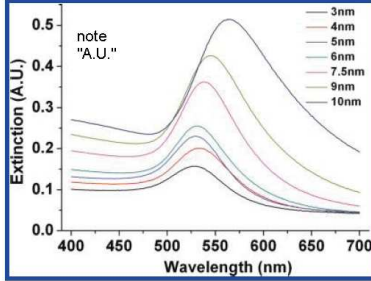
Figure 2: Two promenant figures should be a morphology characterization table and characteristic LSPR spectra with error bars if I can pull it off well-enough.

binding can be monitored in real time with high sensitivity by using simple and inexpensive transmission spectrometry, which measures extinction, the sum of absorption and scattering 3,8-10,41,42. [?]

Thus, changes in the local environment - such as through the presence of an adsorbed species - should cause a shift in $\lambda_m ax$. [?]

The Chemistry of Self-Assembling Films

COMMENT: This section is based on discussion with YS Shon, and attribution should be made for these ideas.

Gold self-assembling films were produced from two sizes of gold particle. The larger particles were Au_{314}, the smaller were Au_{25}. These particles are coated in different organic ligands, which aid their solubility in ethanol (in the case of Au_{314}) and water (in the case of Au_{25}). The ligands are terminated with a carboxy group (COOH) in ethanol and aqueous solutions; in the aqueous Au_{25} solution, ligands may also be terminated with a positively charged carboxy group (COO-).

After the first gold layer is deposited the sample is dipped in an aqueous solution of poly(allyl-amine hydrochloride) (PAH). The PAH bonds to the ligands and allows the next layer to assemble. The aqueous PAH molecules are terminated with amine groups (NH_2) and with positively charged amine groups (NH_3^+). The relative occurrence of the NH_3^+ groups determine the pH of the solution.

In the aqueous Au_{25} solution, the PAH NH_3^+ group favorably bonds to the ligand COOH and COO- groups. The density of the single self-assembled gold layer therefore depends
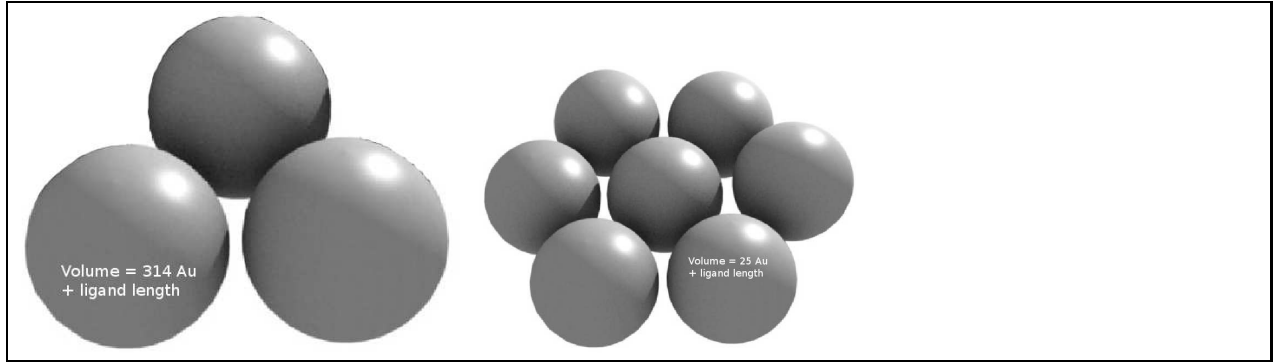
Figure 3: layered gold may be modeled as packed spheres whose packing density depends on radius (approximated) and amount of gold deposited per sphere (known).

(non-linearly) on the pH of the PAH solution, with lower pH (higher ratio of NH_3^+ groups) resulting in higher packing density. The effect of pH on Au_{25} layer density may be studied in this or another paper.

In the ethanol Au_{314} solution, there is an absence of ligand COO- groups. A more neutral pH of the PAH solution allows more bonds between NH_2 and COOH groups.

A model of gold density in Au_{314} and Au_{25} films

The difference in gold density between self-assembling Au_{314} and Au_{25} films can be visually observed. In previous unpublished study, an gold film formed from 8-layers of self-assembled Au_{25} was equivalent in color to a Au_{314} film of approximately 2-4 layers.
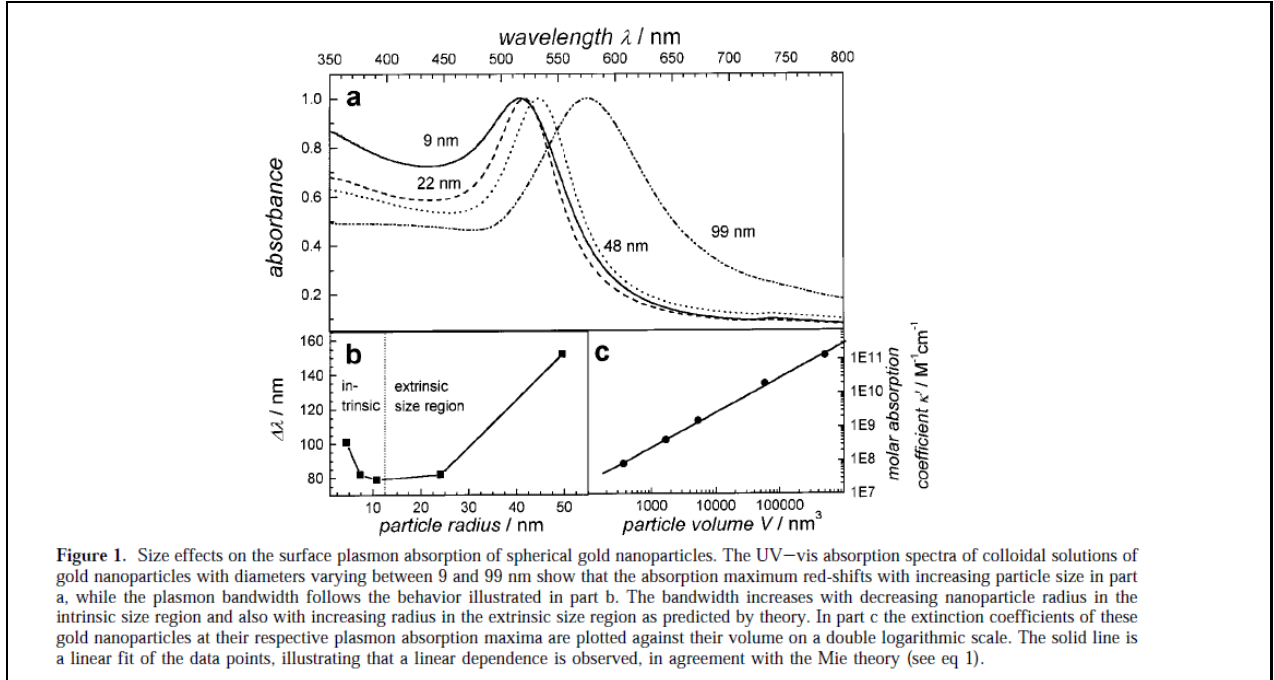
The relationship between color and gold film thickness is a well-documented one, for uniform gold thin films deposited by evaporation, but the color of nano-island films also depend on morphology. The color of nano-island phonons depend not just on thickness, but also size and shape of the islands [?] (cite VanDuyne paper that shows islands up to $99\mu m$ diameter and their resulting LSPR absorption peaks). The size and shape of nano-islands depends on factors that include the initial size of the colloidal gold.

The following comparison of gold density for Au_{314} films of 2-4 layers versus Au_{25} films 8 layers therefore contains a simplified interpretation of the observed color match. We nominally assume that the match of visually observed color implies that the two films, created from the annealing of differently-sized gold particles, are similar in nano-island thickness, shape, and size.

With this assumption in place, a first-order approximation of the relative gold density of Au_{314} and Au_{25} films requires two additional assumptions. First, the average length of the ligands are assumed to be fixed (we neglect that these ligands can easily stretch or shrink). Also, the effect of the pH in the PAH solution on packing density should be considered a second-order effect until demonstrated otherwise.

Figure **??** [image in which the gold particles are modeled as packed spheres]

The approximate ligand length is $2\mu m$ for Au_{314} and approximately $1\mu m$ for Au_{25}. The approximate size of the colloidal gold particles are $2.5\mu m$ for Au_{314} and $1\mu m$ for Au_{25}. Making the assumption that these particles can be modeled as spheres of radius $3\mu m$ for Au_{314} and $1.5\mu m$ for Au_{25} leads to a relative density of 4 nanoparticles of Au_{25} per nanoparticle of

Figure 1. Size effects on the surface plasmon absorption of spherical gold nanoparticles. The UV−vis absorption spectra of colloidal solutions of gold nanoparticles with diameters varying between 9 and 99 nm show that the absorption maximum red-shifts with increasing particle size in part a, while the plasmon bandwidth follows the behavior illustrated in part b. The bandwidth increases with decreasing nanoparticle radius in the intrinsic size region and also with increasing radius in the extrinsic size region as predicted by theory. In part c the extinction coefficients of these gold nanoparticles at their respective plasmon absorption maxima are plotted against their volume on a double logarithmic scale. The solid line is a linear fit of the data points, illustrating that a linear dependence is observed, in agreement with the Mie theory (see eq 1).

Figure 4: Measurements of colloidal gold show a peak absorption dependant on size. A wider distribution of sizes or shapes will produce broadening due to different wavelength centers. This or another article included a table characterizing shape uniformity which would better illustrate.

Au_{314}, which yields an approximate density of $100/314$.

At the first order, three times more layers of Au_{25} should therefore be deposited to yield an equivalent gold mass to the Au_{314} film.

In real application, thermolysis of much more than 8 layers of a film will result in defects of significant density to affect the production of our nanoislands of interest. To produce a thicker film, it is therefore better to use larger Au_{314} particles instead of many layers of Au_{25}.

Size and Shape Distributions and Phonon Absorption Features

The uniformity of the size and shape is expected to correlate with the width of the absorption feature of the resulting sample. A wider distribution of sizes and shapes is expected to produce a broader absorption peak, while a narrower distribution of nanoisland sizes about the average size is expected to produce a sharper absorption feature. This relationship is predicted analytically because identical islands should absorb identically (neglecting second-order effects), producing a maximized peak. Differences among the islands will create phonons that are offset by some amount from the peak wavelength, resulting in a lower and broader peak.

Measurements of colloidal gold (Figure **??** [**?**]) show that peak depends on size and shape [lots of van duyne citations or citations to his original sources].

How to Evaluate the Reproducibility of Nano-Island Samples

The effectiveness of our process control can be evaluated through direct and indirect measurement of the uniformity of the resulting nano-islands. Nano-island size and uniformity can be measured directly through atomic force microscope (AFM) images. Scanning electron microscope (SEM) images may also be used to evaluate size and uniformity, but these SEM was limited to a 10μm minimum window, and could not evaluate the smallest nano-islands (size below $50nm$ (**TBR**)).

Spectral measurements of the nano-island samples will show absorption features which can be used, along with the direct measurements, to indirectly indicate the uniformity of the size distribution of the nano-islands.

> Because there is inherent heterogeneity among individual nanoparticles, each LSPR spectrum is different, revealing the true distribution of resonance wavelengths (20, 98). [**?**]

Determining Size of Nano-islands Through Computer Vision

Results of applying the computer-vision analysis to the nano-island data archive measure the size distribution of several types of nano-islands formed by annealing.

Evaluation Methods for determining Nano-island size

A computer-vision method was selected from the research in section [section number]. Nano-island size was evaluated from AFM measurements of the following nano-island samples.

The size is occasionally split between small islands ($20 - 50nm$) and larger islands ($> 100nm$). Small features appear in the clear annealed glass samples, so it may be that some small features measured by the AFM are features of the glass and not the gold.

Clear glass	0 layers	
2 Au	2 layers	
5 Ag	5 layers	
3 Au 3 Ag	6 layers	
3 Ag 3 Au	6 layers	not sure if there is a difference
(Au Ag)x3	6 layers	
5 Ag 1 Au	6 layers	
5 Au 1 Ag	6 layers	
6 Ag	6 layers	
6 Au	6 layers	
5 Ag 5 Au	10 layers	
5 Au 5 Pd	10 layers	
5 Pd 5 Au	10 layers	not sure if there is a difference
5 Cs Np	unk	pretty sure there's no neptunium
8 Au	8 layers	
1 Au 3 Ag	4 layers	
Au 600	unk	
Others	unk	Need to check AFM log book for file names

Temperature Control, Measurement, and Errors

In-situ measurements require the measurement of temperature and impedance. The impedance is measured at the sample, while the temperature is inferred from thermocouple measurments. Temperature measurments with more than one thermocouple showed that fast heating is uneven across the furnace. Also, during fast heating, impedance measurements of a bare electrode did not match their expected temperature dependance, when the temperature was measured with a nearby 10-mil bare wire K-type thermocouple in air. The glass of the electrode caused the sample temperature to lag up to $100°C$ behind the air temperature during fast heating.

Temperature Control and Temperature Knowledge

Automation was introduced to collect thermocouple temperature measurements at 1Hz sampling, in conjunction with the in-situ sample impedance measurements during heating, thermolysis, and annealing. To quantify the accuracy of thermocouple measurments in predicting sample temperature, impedance was also measured for bare test samples on which no material had been deposited. It was expected that the sample impedance at a given thermocouple temperature measured during fast heating should match the impedence at the same thermocouple temperature measured during slow cooling. Discrepancies in impedance vs. temperature, between fast heating and slow cooling, show accuracy uncertainty in the thermocouple measurement as a predictor of sample temperature.

An automated PID controller was constructed using Arduino microcontroller, a thermocouple daughter-board, and the existing solid-state relay within the Thermolyne furnace.

[Link to the Appendix TBD: Temperature Controller Schematics, BOM, and Code]

Introduction

To allow temperature to be accurately measured (within $50°C$ or better) during fast heating, the heating rate must be controlled during heating. The COTS Thermolyne furnace temperature controller is a simple PID, which when given a setpoint temperature, will approach this temperature as fast as its capabilities allow. To slow the heating to a rate such that the sample temperature may be accurately measured during heating, the PID setpoint was a time-varying function that ramps to the final temperature.

Prior experiments by Toyanath Joshi used a methodical and manual approach of increasing the PID setpoint temperature at the desired rate. A user-controlled ramp was

For the research conducted here, an automated PID controller was constructed using Arduino microcontroller, an open-source hardware thermocouple add-on, and the existing solid-state relay within the Thermolyne furnace. The Arduino microcontroller is well-documented (cite:arduino.cc), and its form factor supports a number of add-on boards("shields") produced by a large number of independant amateur and commercial vendors. The thermocouple "shield" contains four addressable MAX31855 thermocouple digitizers with cold-junction compensation and includes connectors for four K-type thermocouples. The solid-state relay within the Thermolyne furnace was easy to control, as the old PID control could be simply
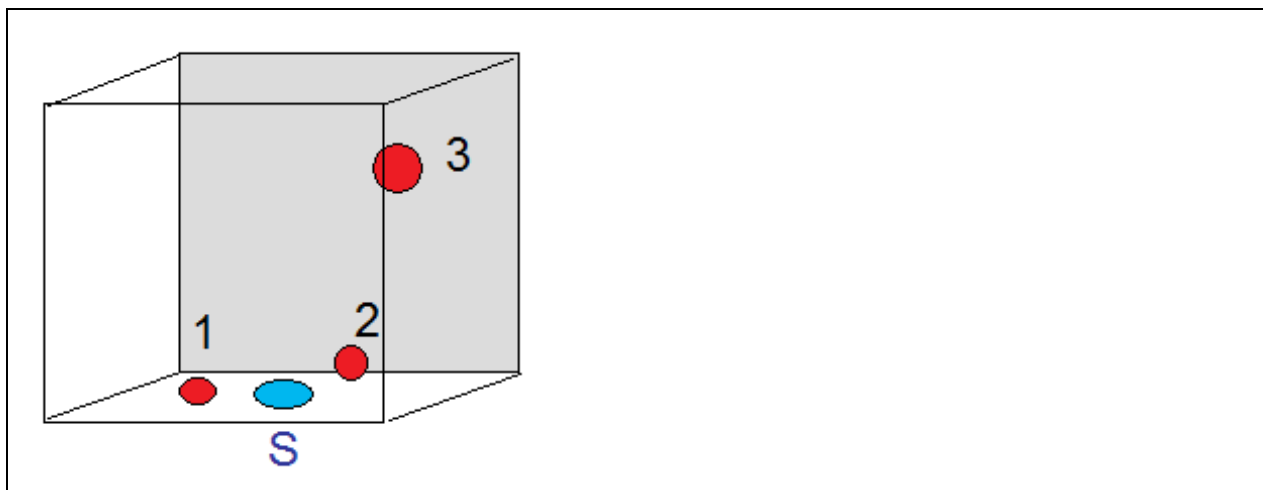
Figure 5: Placement of the three thermocouples and the sample within the furnace used to measure furnace/sample temperature. TC1 is the glass-slide thermocouple, TC2 is a bare TC, TC3 is the furnace TC, and S is the sample.

disconnected and swapped for a new controller (include pic when i'm willing to do disconnect the furnace).

The Arduino has a USB computer interface but also runs stand-alone code independantly of the computer. This means the oven temperature is always controlled by the microcontroller, but the computer interface may be used to request changes to the program running on the controller. The computer is used to set a final setpoint temperature and a rate at which the temperature should be approached. The microcontroller uses these two parameters, along with the current temperature measured from its sensor, to break the ramp into a time-dependant setpoint temperature to pass to a PID algorithm. The PID algorithm decides how best to approach the current setpoint (which will change over time), and over time, the fial setpoint will be reached.

[the PID is better described by code or flow chart than equation]

In the modified temperature controller, any single one of four thermocouples can be used in the PID controller.

Temperature Measurement

Use of multiple thermocouples (Figure **??**) to measure furnace temperature during very rapid heating showed large temperature gradients within the furnace, and that the glass slides on which the samples are mounted slow the heating of the sample.

Three thermocouples were used to measure furnace temperature. The furnace has a heavy gauge K-type thermocouple at the top of the furnace (tc3 in Figure **??**). A bare 10 mil ($254\mu m$) thermocouple (tc2 in Figure **??**) was situated near the bottom of the furnace. A third thermocouple (tc1 in Figure **??**) was attached to a glass microscope slide with a dab of silver epoxy and placed next to the sample.

The IDE sample is responsive to temperature, and a bare IDE should show the same impedance during (fast) heating as it shows during (slow) cooling (Figure **??**). If the temperature measured by a thermocouple results poor overlap of the IDE impedance on the
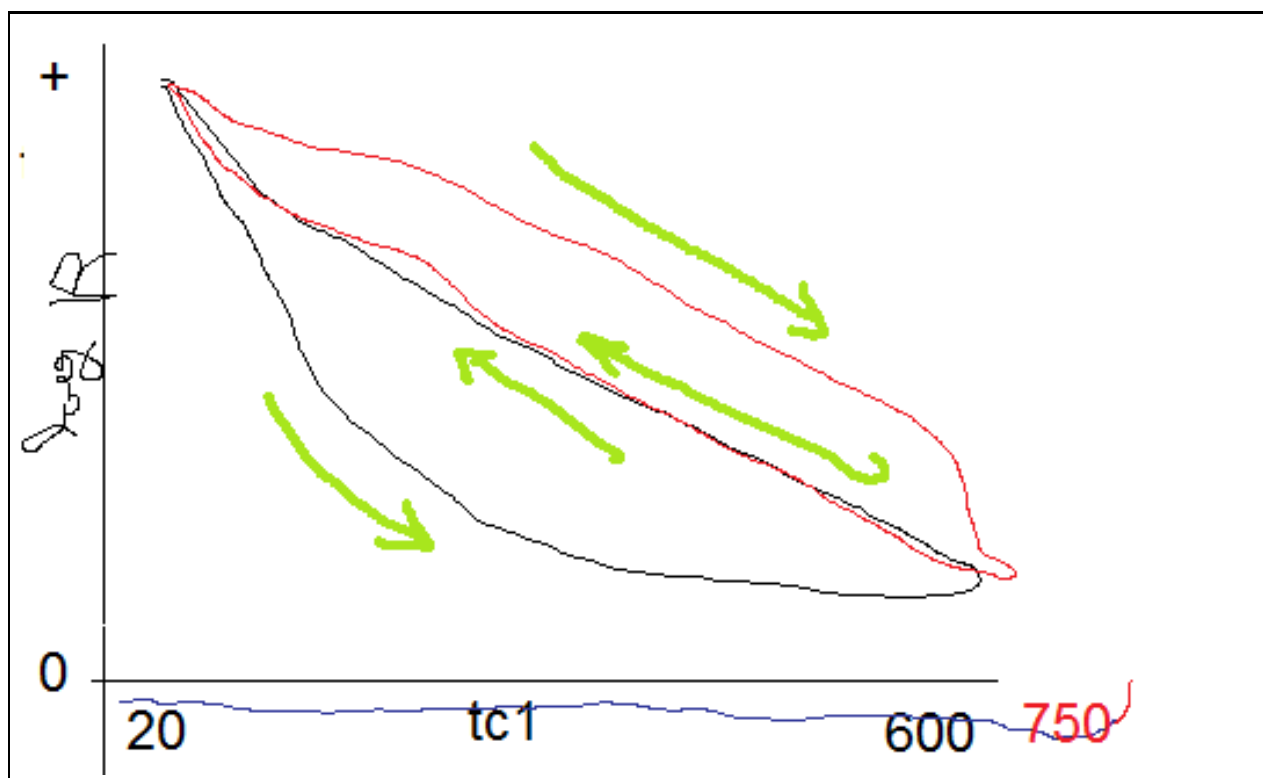
Figure 6: If temperature is accurately measured, the log impedance of the bare IDE sample will match on heating and cooling. If the thermocouple temperature heats faster than the sample, the sample resistance will appear higher on (fast) heating than (slow) cool-down (red trace). If the thermocouple temperature lags the sample temperature on heating, the sample resistance will appear lower on heating than cool-down (black trace). The closer the overlap between heating and cooling, the better the thermocouple matches the temperature seen by the sample.
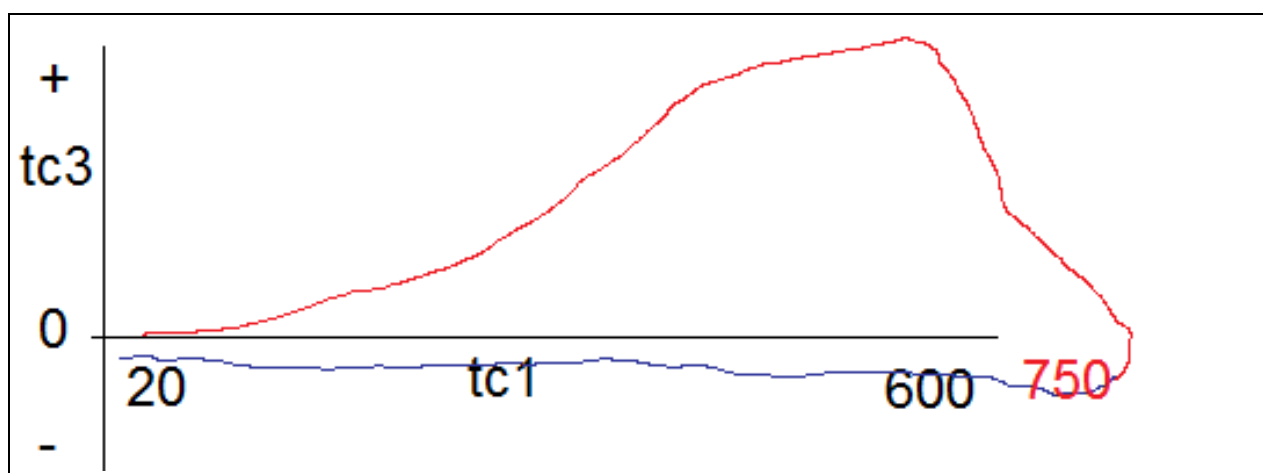
Figure 7: f:plot_tc3_vs_tc1

heating and cooling phases, a temperature error can be inferred. In this way the bare slide can serve as a fourth temperature-sensitive device to confirm that the "sample temperature" inferred from the thermocouple temperature measurements accurately tracks temperature.

The furnace PID controller creates a closed-loop temperature control system, using a single thermocouple to measure the furnace temperature, and a solid-state relay to turn the furnace on and off.

In the modified temperature controller, any thermocouple can be used in the PID controller.

For all furnace tests in Spring 2012, we selected a thermocouple mounted to a glass slide by silver epoxy to close the loop of the PID system. Since the glass-slide TC best tracks the temperature of the IDE sample, it was believed to result in fastest heating. However, because the glass is slower to heat than the air, it can cause a situation in which the furnace overheats.

It was discovered in early testing that the glass slide IDE lags behind the temperature at the top of the furnace by as much as $200°C$ during fast heating of $30°C/min$ (Figure **??**). The build-up of heat and the lag of the glass TC resulted in an overheating of the oven when there is no additional safety measures. A safety measure was introduced into the furnace controller code to turn off the heat if any TC measured greater than $+50°C$ from the furnace setpoint.

For all furnace tests in Summer 2012, we selected a bare thermocouple positioned at the bottom of the furnace (tc2 in Figure **??**) to close the loop of the PID system. Use of the bare TC in the PID system avoids the problem of overheating, and in testing (Section **??**), the glass slide temperature was controlled under fast heating to $625°C$ at a rate of $30°C/min$ with an overshoot of the sample temperature (measured by the glass slide) of just $2°C$ [TBR]. The lack of run-away heating results from the rapid response of the glass slide thermocouple to small changes in air temperature within the furnace, and the mass of the glass slide which causes a slow approach to the final temperature.

## Temperature Errors: Fast Heating is Uneven

Analysis of Furnace Temperature Uniformity Using Three Glass Slide Thermocouples

To test the reproducibility of the glass slide thermocouple, three glass slide thermocouples were made, by affixing a K-type thermocouple to the surface of a glass microscope slide with silver epoxy. A fourth thermocouple was left bare and placed at the bottom of the furnace for use in the PID temperature controller. While the glass slide thermocouple can be used in the PID loop to raise the furnace temperature, it requires a gradient limiter to function safely. The gradient limiter shuts off heating if the temperature between any two thermocouples exceeds a threshold ($50°C$ was used), and is best used with one thermocouple at the top of the furnace (otherwise the gradient is not well sampled).

Because the temperature controller built for this project is limited to four K-type thermocouples, a trade-off was made between fast heating (for which a glass slide TC is used) and complexity (the requirement that the heating gradient be limited). A consequence to using an furnace shut-off is that the heating is no longer at an even rate, and the temperature
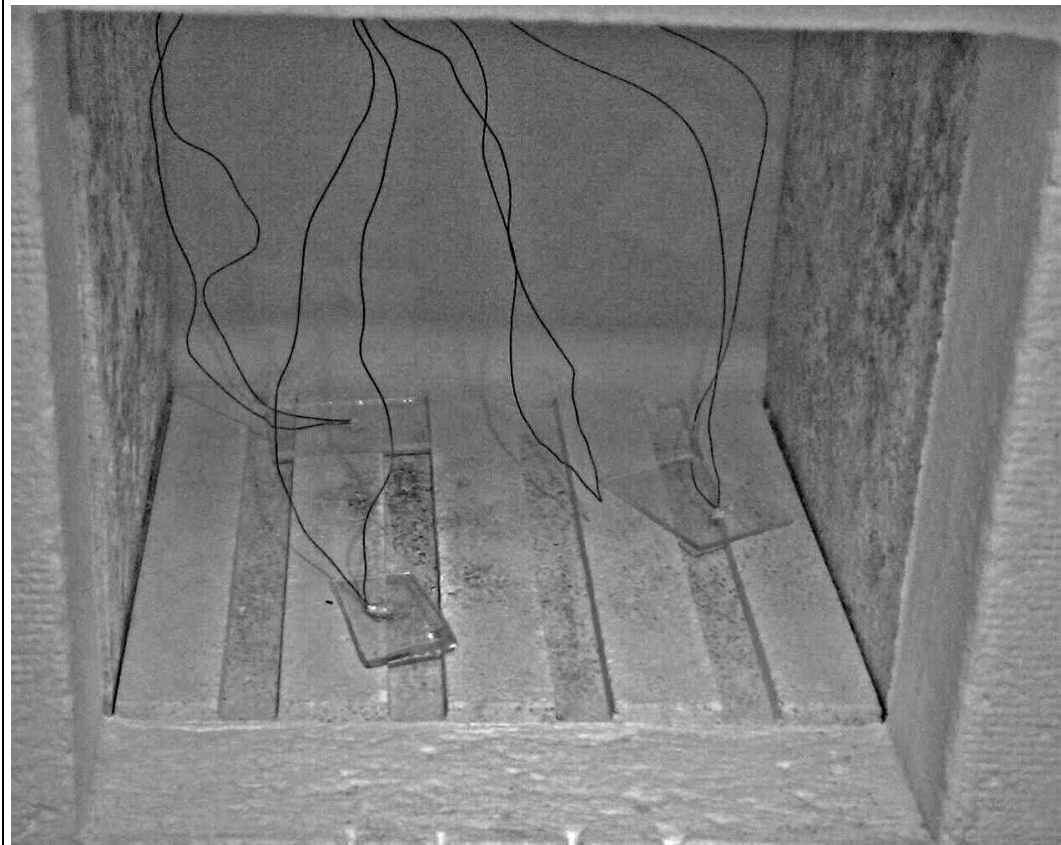
Figure 8: Additional glass slide thermocouples were produced and used to measure the uniformity of the furnace temperature and similarity among glass-slide thermocouples. Three glass slide thermocouples were used for measurement, and a fourth bare TC was used in the PID controller during this test.
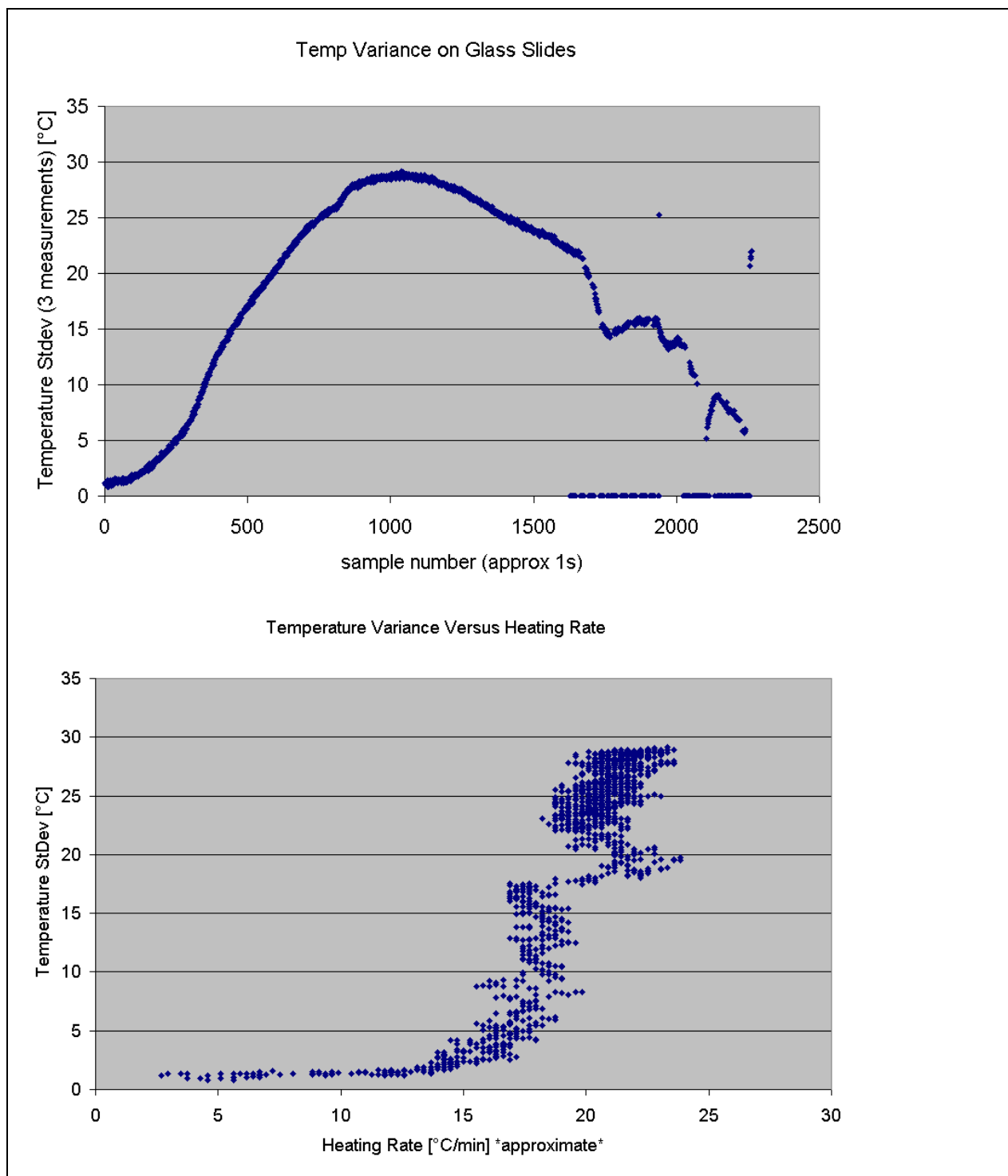
Figure 9: The plot at left shows the standard deviation among the three glass slide thermo-couples during fast heating, which is approximately the magnitude of the bias uncertainty in temperature during heating. The temperature variance versus heating rate is plotted at left. The magnitude of the temperature gradients across the base of the furnace are non-linearly proportional to temperature.

characterization emphasizes errors (Figure "shutoff emphasizes errors in Au25 test").

Results of the glass slide thermocouple uniformity measurement shows that three glass slides placed across the bottom of the furnace, when heated at a rate $25^{circ}C$ per second, show a disagreement of $X°C$ at the fastest rate of heating (Figure "three slides result").
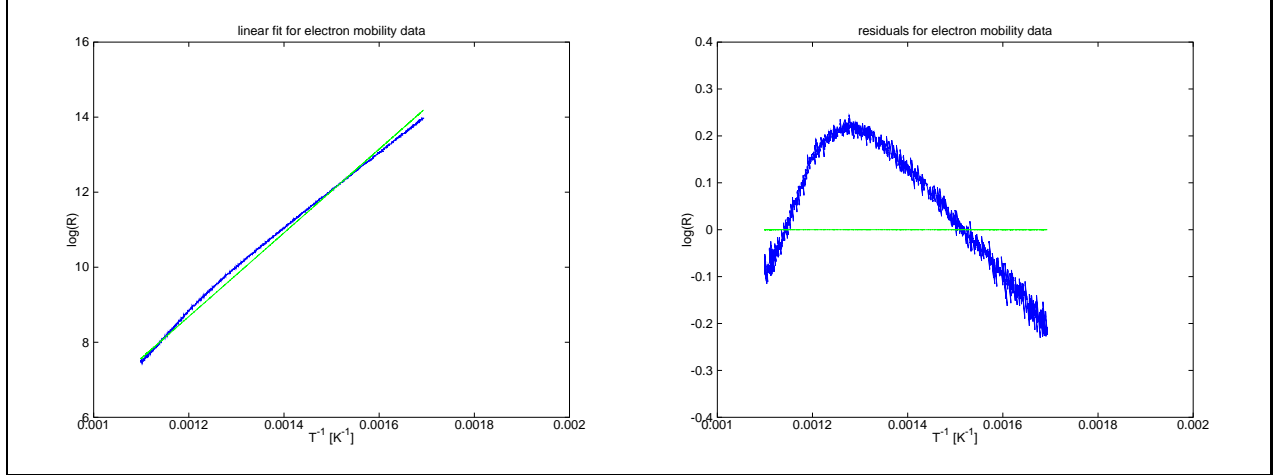
Figure 10: During cool-down of the sample, the impedance versus temperature measurements are well-sampled, and can be used to solve for electron mobility. $\frac{\epsilon}{k} = 1.1e + 04K$, $\epsilon = 0.96eV$, $R_0 = 9.1e - 3\Omega$. Error bars are needed, and will have magnitude at least proportional to the fit residuals.

In-Situ Transport Measurements and Complex Impedance

Electron Transport Measurement using Complex Impedance

A four-point impedance measurement measures complex impedance of the IDE sample under test (device under test, or DUT). Impedance measurements follow a temperature dependence derived from models of electron transport under an AC potential. Complex impedance and temperature measurements are used to solve electron mobility under the AC electron transport model detailed below. Temperature measurements were limited to those measurements taken during cool-down of the DUT, since temperature measurements during fast heating of the sample carry very large errors. Measurements of impedance over temperature during cool-down (FIGURE "cooldown_residuals") were identical within uncertainties for the Au$_2$5 sample (JD04) and a bare IDE sample (JD05), and electron mobility will be identical. Electron mobility calculated for the Au$_2$5 (JD04) sample was $\frac{\epsilon}{k} = 1.1e + 04K$, $\epsilon = 0.96eV$.

Introduction: Measurement of Complex Impedance

DC resistance measurements of the electrode show only its insulating properties, as the glass substrate is a poor conductor and the IDE is a weak capacitor, so AC resistance is measured. AC resistance in the IDE samples follows the temperature-dependent electron mobility.

$$R = R_0 \cdot e^{\frac{\epsilon}{k \cdot T}} \tag{1}$$

This equation can be rearranged into a linear equation to solve for ϵ.

$$ln(R) = \frac{\epsilon}{k}\frac{1}{T} - ln(R_0) \tag{2}$$

$\frac{\epsilon}{k}$ and $ln(R_0$ are found by least-squared fit of the linear portion of the data.

The temperature range observed is between $295K$ and $900K$,

Sample resistance (a parallel AC resistance) is typically high for the sample under test, this resistance changes when the sample is heated and the polymers are burned off.

The resistance R_p of a high-resistance sample can be measured from the complex impedance (Z, θ) by Equation **??**. Use of the parallel resistance R_p is justified at high sample resistance because the series resistance R_s of the test leads and contacts are orders of magnitude smaller.

$$R_p = \frac{Z}{cos(\theta)} \tag{3}$$

Typical values for complex impedance measured by the auto-balancing bridge method via an Agilent 82XX LCR meter are as follows.

$$(Z, \theta, \nu, T) = (15M\Omega, -89.9°, 1kHz, 22°C) \tag{4}$$

$$(Z, \theta, \nu, T) = (800k\Omega, -88°, 45kHz, 22°C) \tag{5}$$

This result shows that the R_p "resistance" component (which is Z divided by $cos(-89°)$) is immeasurably high at low frequencies and low temperature. It is only at higher temperatures that R_p drops to the measurable range, and this occurs at about $250°C$ when the impedance phase angle θ drops from $-89.9°$ towards $0.1°$.

During the burn-off of the polymers, the parallel resistance may drop to under 100 ohms, which requires a four-point measurement to compensate for the series resistance test lead impedance. A four-point measurement is necessary because the test leads have been reported (AD5933) to have up to kilo-ohm impedance when measuring low sample resistance.

Post-Processing Measurement Methods Discussion

AFM

SEM

LSPR

Gold Nano Island Preparation

Preparing Gold Slides

Preparation of Gold Nanoparticle Solution

The preparation of the gold nanoparticle solution requires about a week of preparation to yield the 10 mL of Au_{314}.

Layering the Samples

To deposit the self-assembling multilayers on a glass electrode, the following steps are

- First Day

  - An aqueous solution of poly(allylamine hydrochloride) (PAH) is prepared, adding 10mg PAH to 10mL nanopure water, for use on Day Three.

  - 1.0mL methanol is added to 0.1mL triethyl 3-mercaptopropylsilane in a 5mL vial.

  - 0.1mL of nanopure water is added to the solution. (The triethyl 3-mercaptopropylsilane will react with the water and the solution becomes cloudy).

  - The IDE is placed in the solution for 24 hours.

  - *Note*: it is important not to leave the IDE for more than 24 hours, or the IDE will acquire a thick deposited coating.

- Second Day

  - The IDEs are placed in clean 5mL vials.

  - Methanol is added to the vials and the samples are sonicated in an ultrasonic bath.

  - The methanol wash is removed, and the washing process is repeated 2 more times.

  - After the third ultrasonic wash, the samples are gently dried under a stream of nitrogen gas or air.

  - After drying, gold nanoparticle solution is added to each vials, enough to cover the IDE.

  - The IDEs are left in the nanoparticle solution overnight.

- Third Day

  - A work station is prepared with an ultrasonic bath, Pasteur pipettes, nanopure water, ethanol, PAH solution, and several spare 20mL vials for containing waste or re-used liquids.

  - for layer = 2:10

    * The gold nanoparticle solution is removed from each vial using Pipette A and placed in a 20mL vial for reuse.

    * A washing solution of nanopure water (Au_{25}) or ethanol (Au_{314}) is added to each vial using Pipette A, and the vials are placed in an ultrasonic bath.
      Washing the IDE by inverting the vials is not recommended, as this breaks bonding wires. An ultrasonic bath prevents damage to the wire bonds.

    * If the nanoparticle solution is Au_{314}, the ethanol is removed with Pipette A, nanopure water added, and the vials are again placed in the ultrasonic bath.

    * The nanopure water is removed from the vial (for Au_{314} and Au_{25}) using Pipette A.

    * The PAH solution is added to each vial using Pipette B and the vials are left to stand for 5 minutes.

17

* The PAH solution is removed from the vials using Pipette B, nanopure water is added with Pipette B, the vials are placed in an ultrasonic bath, and the nanopure water is removed using Pipette B.
* If Au_{314}, then add ethanol using Pipette A and place the vial once more into the ultrasonic bath, and the ethanol is removed with Pipette A.
* If this layer is not the last layer, the Au_{314} or Au_{25}) solution is added to the vials using Pipette A, and the vials are left to stand for 5 minutes.
  - end for loop (next layer)
  - The IDEs are gently dried under a stream of nitrogen gas or air, and placed in a vacuum desiccator in the dark, for storage.

Bonding and Baking

Attaching Bonding Wires for Four-Point Impedance Measurement

[Discussion and images of two methods of bonding used in this study]

Electron Transport Measurements of Au$_{25}$

In-situ impedance measurements of Au_{25} are indistinguishable from measurements of a bare electrode.

Setup/Procedure

Impedance, Temperature Measurements, AFM/SEM Images, LSPR

Conclusions

Electron Transport Measurements of Au$_{314}$

In-situ impedance measurements of Au_{314} shows a feature during heating.

Setup/Procedure

Impedance, Temperature Measurements, AFM/SEM Images, LSPR

Conclusions

Appendix A: Furnace Control and Temperature Measurement

A furnace controller was designed to limit the heating of the sample to improve temperature measurement accuracy.

Source code for the furnace controller, and version-locked libraries for PID control and MAX31855 Thermocouple reader, are kept at a `https://github.com/John-NY/Arduino_Furnace_Controller_PID`.

Furnace Controller block diagram

Furnace Controller Bill of Materials

The furnace temperature controller was programmed on hardware consisting of an Arduino microcontroller and McLaughlin Engineering four channel MAX31855 K-type thermocouple interface board (Arduino "shield").

A PID implementation was optimized for switch-type relays, that minimizes the number of switch events by limiting switch events to those of 1 second duration or longer. Lifespan of a mechanical switch-type relay is measured in switch events, so minimizing the number of switch events will prolong life of the relay and minimize the likelihood of relay failure.

- McLaughlin Engineering - MAX6675, MAX31855 breakout

  Link: `http://ryanjmclaughlin.com/wiki`

  Dimensions: Arduino Shield

  Chip: MAX31855, TXB0104

  Voltage: 5V, 3.3V

  Header: 2 - 1x6 0.1" Pitch, 2 - 1x8 0.1" Pitch

  Fixturing: Matching holes to Arduino

- Omega Type-K Thermocouple

  Bare Wire 0.010 K-type

  Mini Connector K-type

- Arduino Microcontroller

  Link: `http://arduino.cc`

Furnace Controller Schematic Block Diagram

The temperature controller was

Arduino Code: Furnace Controller PID and Serial Ramp